Activation of sub-3 nm organic particles in the particle size magnifier using humid and dry conditions

Rörup, Birte

2022-03

Rörup , B , Scholz , W , Dada , L , Leiminger , M , Baalbaki , R , Hansel , A , Kangasluoma , J , Manninen , H E , Steiner , G , Vanhanen , J , Kulmala , M & Lehtipalo , K 2022 , ' Activation of sub-3 nm organic particles in the particle size magnifier using humid and dry conditions ' , Journal of Aerosol Science , vol. 161 , 105945 . https://doi.org/10.1016/j.jaerosci.2021.105945

http://hdl.handle.net/10138/345542
https://doi.org/10.1016/j.jaerosci.2021.105945

Journal of Aerosol Science 161 (2022) 105945

Contents lists available at ScienceDirect

Journal of Aerosol Science

journal homepage: www.elsevier.com/locate/jaerosci

Activation of sub-3 nm organic particles in the particle size magnifier using humid and dry conditions

B. Rörup [a,*], W. Scholz [b], L. Dada [a,c,d], M. Leiminger [b,e], R. Baalbaki [a], A. Hansel [b,e], J. Kangasluoma [a], H.E. Manninen [f], G. Steiner [g], J. Vanhanen [h], M. Kulmala [a,i,j,k], K. Lehtipalo [a,l]

[a] Institute for Atmospheric and Earth System Research/Physics, Faculty of Science, University of Helsinki, Finland
[b] University of Innsbruck, Innsbruck, Austria
[c] EPFL, Extreme Environments Research Laboratory, Ecole Polytechnique Fédérale de Lausanne (EPFL) Valais Wallis, Sion, 1951, Switzerland
[d] Laboratory of Atmospheric Chemistry, Paul Scherrer Institute, Villigen, 5232, Switzerland
[e] IONICON Analytik, Innsbruck, Austria
[f] Helsinki Region Environmental Services Authority HSY, FI-00066, Helsinki, Finland
[g] GRIMM Aerosol Technik Ainring GmbH & Co KG, Ainring, Germany
[h] Airmodus, Helsinki Ltd., Finland
[i] Joint International Research Laboratory of Atmospheric and Earth System Sciences, School of Atmospheric Sciences, Nanjing University, Nanjing, China
[j] Aerosol and Haze Laboratory, Beijing Advanced Innovation Center for Soft Matter Sciences and Engineering, Beijing University of Chemical Technology (BUCT), Beijing, China
[k] Faculty of Geography, Lomonosov Moscow State University, Moscow, Russia
[l] Finnish Meteorological Institute, Helsinki, Finland

ARTICLE INFO

Keywords:
Particle size magnifier
Condensation particle counter
Calibration
Detection efficiency
Sub-3 nm aerosols

ABSTRACT

The accurate measurement of aerosol particles and clusters smaller than 3 nm in diameter is crucial for the understanding of new particle formation processes. The particle counters used for measuring these particles are typically calibrated with metal or salt particles under dry conditions, which does not always represent the field conditions where these instruments are later used. In this study, we calibrated the A11 nano Condensation Nucleus Counter (nCNC), consisting of the PSM (Particle Size Magnifier) and a laminar flow butanol based CPC (Condensational Particle Counter), with well-defined biogenic oxidation products from β-caryophyllene oxidation and compared it to a calibration with tungsten oxide under the same conditions. The organic particles were detected less efficiently than the inorganic ones. This resulted in a higher cut-off size for β-caryophyllene oxidation products than for tungsten oxide. At the same PSM settings, the cut-off size for tungsten oxide was 1.2 nm and for β-caryophyllene oxidation products 1.9 nm. However, repeating the calibration of the biogenic particles at 13% relative humidity at 31°C, increased their detection efficiency in the PSM, increasing the cut-off diameter to 1.6 nm.

Additionally, we present a comparison of the ion concentrations measured with the PSM and the NAIS (Neutral Cluster and Air Ion Spectrometer) during new particle formation experiments in the CLOUD (Cosmics Leaving Outdoors Droplets) chamber. In these experiments, we produced particles from different organic precursors, such as α-pinene, β-caryophyllene and isoprene, as well as iodine. This way, we could determine the shift in cut-off diameter of the PSM for several

* Corresponding author.
E-mail address: birte.rorup@helsinki.fi (B. Rörup).

https://doi.org/10.1016/j.jaerosci.2021.105945
Received 31 August 2021; Received in revised form 22 December 2021; Accepted 24 December 2021
Available online 3 January 2022

different atmospherically relevant chemical compounds and compare it to the laboratory calibrations. We saw a diameter shift for the organic precursors of +0.3 nm in the PSM compared to the NAIS. These two approaches agreed well with each other and show that it is important to know the chemical composition of the measured particles to determine the exact size distribution using a supersaturation scanning method.

1. Introduction

Atmospheric aerosol particles can cause human health deterioration (K.-H. Kim et al., 2015) and significantly impact the global climate directly by scattering the sunlight and indirectly by affecting cloud formation (Albrecht, 1989; Bauer et al., 2012). While some aerosol particles are directly emitted from sources such as biomass burning, volcanoes or sea spray, most aerosol particles are created in the atmosphere due to clustering of vapour molecules (Merikanto et al., 2009). These clusters will grow by condensation and form aerosol particles. This process is called new particle formation (Kulmala et al., 2013). Accurate measurements of ultrafine particles in the size range between 1 and 10 nm are essential for a detailed understanding of this process and quantifying the new particle formation rate and growth rates (Kulmala et al., 2012). However, quantitative measurements in this size range remain a challenge (Kangasluoma et al., 2020).

Condensation particle counters (CPC) measure aerosol particles optically after growing them through condensation of a working fluid into optically detectable sizes (McMurry, 2000). CPCs are essential for many studies since they can measure both neutral as well as charged particles down to extremely small number concentrations of 1 particle per cm^{-3}. They are frequently used e.g. in atmospheric field measurements (Brilke et al., 2019; McMurry, 2000; Z. Wang et al., 2017; Woo et al., 2001), laboratory studies (Attoui, 2018; Picard et al., 2019; Wlasits et al., 2020), as well as monitoring indoor air quality (Patel et al., 2020; Stabile et al., 2016) and vehicular emissions (X. Wang et al., 2010). There are different types of CPCs, which use different working fluids like water, butanol and diethylene glycol (DEG). The working fluid directly affects the activation efficiency of particles and thus the size where 50% of particles compared to the plateau value are detected, which is defined as the cut-off of a CPC. Iida et al. (2009) concluded that DEG could be used to achieve very low cut-off sizes without homogenous nucleation. Since then, several so called 'low cut-off' CPCs, which are using DEG have been developed (Jiang et al., 2011; Kuang et al., 2012; Wimmer et al., 2013). DEG is also sometimes used in particle size magnifiers (PSM), which were first introduced by (Kogan et al., 1960) and later further developed by e.g. Okuyama et al. (1984), Seto et al. (1997), C. S. Kim et al. (2003) and Ito et al. (2011). Airmodus Ltd. commercialised the A11 nano Condensation Nucleus Counter (nCNC), which consists of a PSM, an aerosol pre-conditioner that uses DEG to grow particles as small as 1 nm to approximately 90 nm, and a butanol based CPC (Vanhanen et al., 2011). The Airmodus PSM is based on the design of Sgro et al. (2004). The flow rates within the Airmodus PSM, which affect the supersaturation and thus the cut-off diameter, can be changed periodically to measure the particle size distribution between 1 and 3 nm (Lehtipalo et al., 2014).

Previous studies show that the heterogeneous nucleation processes responsible for particle activation inside the particle counters are dependent on the chemical composition of the sample aerosol (Iida et al., 2009; Kangasluoma et al., 2014; Wlasits et al., 2020). Particle counters are usually calibrated with metal or salt particles under dry conditions (Wiedensohler et al., 2018; Yli-Ojanperä et al., 2012). This causes uncertainties when measuring atmospheric particles, especially those of organic origin, since the chemical composition is significantly different. According to a modelling study, the cut-off diameter can shift to bigger sizes for organic particles compared to inorganic ones, because of the reduced amount of hydrogen bonding sites (Keshavarz et al., 2020). This means that the diethylene glycol based particle counters are probably not as sensitive to organic particles as they are to inorganics. A previous study on the PSM's detection efficiency towards particles of different composition using limonene and tungsten oxidation products (Kangasluoma et al., 2014) supports this. However, there is lack of knowledge regarding other atmospherically relevant organic compounds. Here we used β-caryophyllene (BCY) for the PSM calibration, because it produces HOMs (highly oxygenated organic compounds), which are frequently observed in the atmosphere (Ehn et al., 2014; Jokinen et al., 2016). HOMs are also believed to take part in particle formation and growth processes (Kirkby et al., 2016; Lehtipalo et al., 2018). Additionally, we investigated the humidity dependency of the PSM detection efficiency, which have not been quantified before. These experiments were done under well-defined laboratory conditions to provide further information of the particle activation in the PSM.

We also used data from the CLOUD (Cosmics Leaving OUtdoor Droplets) chamber experiments at CERN (Kirkby et al., 2011) to confirm our laboratory results. During these campaigns, several nucleation experiments were performed in the chamber with different inorganic and organic precursor gases and their mixtures. During those experiments, the PSMs and a Neutral Cluster and Air Ion Spectrometer (NAIS) (Mirme et al., 2013) measured the particle size distribution from the chamber in parallel (Wagner et al., 2016). The NAIS measurements are not affected by chemical composition, therefore comparing those instruments can provide additional information about the sensitivity of the PSM to different particle compositions (Dada et al., 2020).

In the present study, we aim to determine the PSM cut-off diameter for atmospherically relevant organic particle mixtures relative to standard calibration compounds and further explore how the measurements are affected by changes in relative humidity. The ultimate goal is to improve future measurements and data analysis of sub-3 nm aerosol particles and our general understanding of how composition affects heterogeneous nucleation and activation probabilities.

2. Methods

2.1. Instruments

2.1.1. Particle size magnifier

We used the Airmodus A11 Nano Condensation Nucleus Counter (nCNC) to measure the aerosol particle number size distribution between 1 and 3 nm. The nCNC consists of the A10 PSM and the A20 CPC. The PSM uses diethylene glycol (DEG) as the working fluid, which saturates the flow in the saturator and later condenses on the aerosol particles in the growth tube and grows these particles to sizes the CPC can detect. The cut-off diameter of the PSM can be decreased by increasing the flow through the saturator. This increases the supersaturation inside the growth tube and smaller aerosol particles are activated. The flow rate through the saturator can be adjusted between 0.1 and 1.3 L per minute (lpm), which corresponds to a particle activation range of about 1–3 nm. The saturator flow can be set to scanning, stepping or fixed mode, according to the preferences of the user. For our experiments, the saturator flow rate was set to scanning mode. This means, that the saturator flow rate increases linearly within 2 min from 0.1 lpm to 1.3 lpm and then decreases in the same time period to 0.1 lpm. The PSM must be calibrated before use to determine which particle sizes are activated at which saturator flow rate. In addition to the saturator flow rate, the cut-off diameter of the PSM is determined by the temperature difference between the saturator and the growth tube. Higher temperature difference leads to a higher supersaturation and a lower cut-off diameter. However, if the temperature difference is too high, DEG nucleates homogenously, which causes false background counts (Vanhanen et al., 2011).

Here, we calibrated the PSM with positive BCY oxidation products at two different supersaturation settings. In the low supersaturation setting, the saturator temperature was 78°C and the growth tube temperature was 2°C. No homogeneous nucleation was observed inside the PSM and the settings were the same as during the calibration with tungsten oxide (WOx). In the higher supersaturation setting, the saturator tube temperature was increased to 80°C and the growth tube temperature stayed the same. At this setting, homogeneous nucleation lead to a particle concentration of about 5 cm^{-3} in the PSM at the highest saturator flow rate. This is similar to the settings used at SMEAR II station to detect atmospheric clusters (Sulo et al., 2020).

The settings that were used during our calibration are listed in Table 1. Additionally, we also did experiments with increased relative humidity and fixed particle size at 1.7 nm, where the saturator temperature was set to 76°C, 78°C, 80°C and 82°C. This setup is explained in chapter 2.2.

2.1.2. ioniAPi-TOF

During the calibration with BCY, we used an atmospheric pressure interface time-of-flight (APi-TOF) mass spectrometer from IONICON Analytik, referred to as the ioniAPi-TOF, to measure the chemical composition of the charged particles after they were size selected by the uDMA (Fig. 1A). These are sampled from atmospheric pressure and transferred through three pressure stages via hexapole ion guides and ion optics into the vacuum (of about 10^{-6} mbar) of the mass analyser. Here, the ioniAPi-TOF has a mass resolution (m/Δm) of about 6000. The data of the positive ion mode was used for this analysis (Leiminger et al., 2019).

We calibrated the mass axis of the ioniAPi-TOF with positive Tetraheptylammonium bromide monomers and dimers. Afterwards, the mass axis was automatically corrected using typical BCY oxidation products when there were small axis shifts over time by non-constant lab temperature. This gives us a well calibrated mass axis up to masses of m/z 800, above that the mass axis can deviate slightly.

2.1.3. Neutral Cluster and Air Ion Spectrometer

The Neutral Cluster and Air Ion Spectrometer (NAIS) is a multichannel ion mobility spectrometer that can measure the number size distribution of charged particles (ions) of both polarities as well as total (naturally charged and neutral) particle concentration. The NAIS consists of two parallel differential mobility analysers (DMA), which measure the positive and negative ions of mobility diameters in the range of 0.8 nm–40 nm (Manninen et al., 2016; Mirme et al., 2013). During the CLOUD experiments used in this study, it was set to measure only ions. The uncertainty of the ion concentration measurements of the NAIS is less than 10%, which makes it a good reference instrument in this study (Wagner et al., 2016).

2.2. β-caryophyllene calibration setup

The BCY oxidation products were created in a continuous Teflon bag reactor with the dimensions 98x47x2 cm and a reaction time of 11 s. The temperature in the bag was 31°C during the experiments. The setup is presented in Fig. 1A. We used 10 mlpm dry (RH = 0%) compressed air as carrier flow to inject BCY from its glass bubbler into the bag. We also used 4 lpm compressed air through 2 UVP ozone generators from Analytik Jena to introduce ozone into the bag. The bypass flow was 31 lpm. The airflows containing ozone and BCY were mixed upon entry into the bag. The total flow through the bag was 35 lpm. The conditions in the bag were constantly

Table 1
PSM settings during the calibration.

PSM Saturator temperature	PSM Growth tube temperature	PSM inlet temperature	CPC Saturator temperature	CPC Condenser temperature
78°C or 80°C	2°C	40°C	39°C	20°C

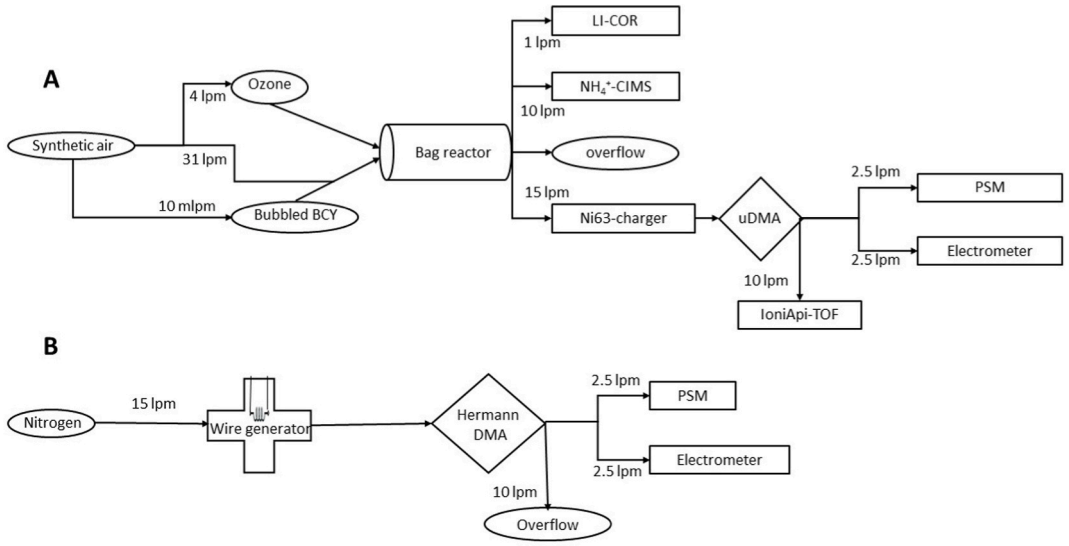

Fig. 1. Schematic of the β-caryophyllene calibration setup (A) and tungsten calibration setup (B).

monitored by the NH_4^+-CIMS, an ammonium chemical ionisation mass spectrometer (Hansel et al., 2018), based on the ion source designed by Breitenlechner et al. (2017) to confirm that there are no contaminations in the bag and to measure the BCY concentration. We used 30 ppb BCY, which reacted with 200 ppb ozone, which was measured at the overflow by the ozone monitor 49C from Thermo Environmental Instruments, for the calibration.

The generated particles were charged with a Ni63 charger and then size selected according to their electrical mobility by a high-resolution uDMA (Steiner et al., 2010). We calibrated the PSM with positively charged BCY oxidation products and compared it to the negatively charged tungsten oxide calibration. It was not possible to create the necessary amount of negatively charged particles in this setup. It should be noted, that there can be a difference in the detection efficiency for particles with different polarities, because charge can affect the heterogenous nucleation probability by affecting the seed-adsorbate interactions (Keshavarz et al., 2020). For Tungsten oxide, earlier experiments have shown that the difference is −0.15 nm in the PSM cut-off size between negatively to positively charged particles, probably due to organic contaminations below 1.5 nm in the positive mode (Kangasluoma et al., 2014).

Ten lpm of the sample flow were directed to the ioniAPi-TOF for mass spectral analysis confirming the chemical composition of the measured particles. The remaining 5 lpm were evenly split between the PSM and the reference instrument, a custom built faraday cup electrometer with a noise level of 10^{-16} A, based on the design presented by Winklmayr et al. (1991). The setup was constructed in a way that the losses in the PSM inlet are the same as the ones in the electrometer inlet. With this setup, we managed to generate a charged particle concentration, which varied between 500 and 8000 cm^{-3} for charged particles between 1 and 2.5 nm for the calibration.

During the calibration, the PSM is set to scanning mode, while the DMA is in fixed mode so that the PSM and electrometer are measuring just one size bin at the time. This is repeated for several DMA settings to get the desired size range. The PSM can be compared to the electrometer to get the relation between the saturator flow and the cut-off diameter of the PSM, as well as the detection efficiency. The calibration was done under dry conditions.

Additionally, we did experiments with increased humidity up to 10 g m^{-3} inside the Teflon bag, which corresponds to a relative humidity of 30% at 31°C, by humidifying part of the carrier flow with a temperature controlled water vapour saturator. The humidity was measured by an infrared gas analyser from LI-COR Biosciences (LI-840A).

2.3. Tungsten calibration setup

We calibrated the PSM with tungsten oxide particles (WOx) using the setup explained in Kangasluoma, Attoui, et al. (2015), which can be seen in Fig. 1B. A wire generator (Peineke et al., 2006; Schmidt-Ott et al., 1980) with tungsten wire is heated by applying a high current to it until it produces supersaturated vapour. The vapour cools down when it is carried away from the wire by the carrier flow, condenses and forms clusters. In our case, these clusters are naturally charged and can be classified by their electrical mobility. For the classification, we used a high resolution Herrmann DMA, which was connected to a positive voltage to classify negatively charged particles (Kangasluoma et al., 2016). After the classification, the flow is split evenly between the reference instrument, an electrometer (TSI 3068B), and the PSM. With this setup, we can generate high concentrations of monodisperse particles between 1 and 3 nm. The calibration was done under dry conditions and the same way as it is described in chapter 2.2.

2.4. Comparison to NAIS during the CLOUD experiments

The CLOUD chamber at CERN is a 26.1 m^3 stainless steel cylinder operated in continuous mode. It is used to study nucleation processes in well controlled, simulated environments (Duplissy et al., 2016; Kirkby et al., 2011; Wagner et al., 2017). A nucleation event is simulated by injecting precursor gases like α-pinene, which reacts with oxidants and starts forming particles. Depending on the experiment, different precursors or their mixtures are used. The experiments are repeated at different mixing ratios of precursors, different temperatures and relative humidities. The experiment is continued until a steady state is reached or particles have reached large enough sizes, then they are cleaned out and the chamber is prepared for the next experiment. The experiments used in this study are from CLOUD10, CLOUD11 and CLOUD13 and they were all done in the Galactic Cosmic Rays mode (GCR), meaning that ions were produced in the chamber by natural galactic cosmic rays and no additional ionisation was used.

During the experiments, several instruments are continuously extracting samples from the chamber. We compared the PSM data to the NAIS data during new particle formation experiments, using different precursor mixtures to determine the diameter shift of the PSM for each particle composition. The NAIS can be operated in ion mode, where it only measures the naturally charged particles, and total mode, where the neutral particles are charged with a corona needle, so they can be measured as well. In total mode, the particles below 2.5 nm are affected by the charger ions from the corona needle (Manninen, 2011) and therefore a direct comparison between the PSM and NAIS in total mode is not possible (Kangasluoma et al., 2013).

Therefore, we used a setup described in Wagner et al. (2017) to compare the two instruments. This setup consists of two PSMs in scanning mode sampling from the same line. One had an ion filter in front of the inlet, which removed all charged particles below 10 nm (Kangasluoma, Franchin, et al., 2015). Thus, this PSM was only measuring neutral particles (PSM_n). The other PSM was measuring the total particle count, charged and neutral particles (PSM_t). The ion concentration below 3 nm can thus be calculated from the difference between the two PSM measurements (Dada et al., 2020).

$$N_{ion} = N_{PSM_t} - N_{PSM_n} \tag{1}$$

This gives us the ion concentration from the PSM, which can be compared to the total ion concentration from the NAIS, which was calculated by summing up the ion concentrations starting from different size channels. During the CLOUD experiments, we regularly perform experiments also in neutral conditions. During neutral experiments, all ions in the chamber are removed by a high voltage field cage (Kirkby et al., 2011). These experiments were used to verify that the PSM_t and PSM_n measure the same concentration during neutral conditions. By performing this check, we ensure that the only difference between the number concentration measured by the two PSMs is the result of ions trapped by the ion trap in front of PSM_n.

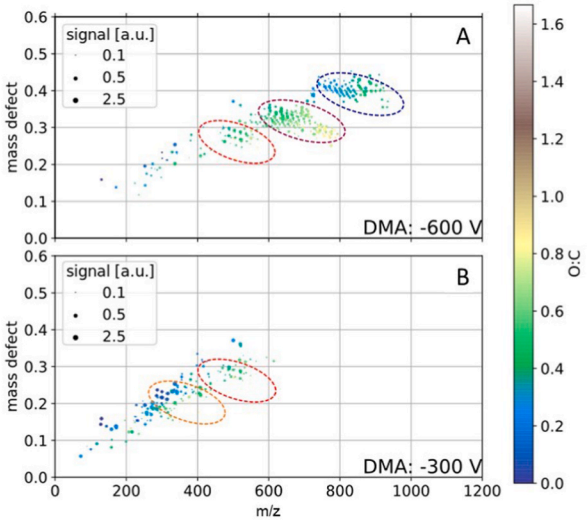

Fig. 2. The mass defect for the positively charged BCY oxidation products, produced for the calibration at DMA voltage −600V (A) and −300V (B), which corresponds to classified particles of 1.6 nm and 1.2 nm in mobility diameter, respectively. It is coloured by O:C ratio and the size of the points is log-scaled with the signal strength at the exact mass. The monomers, dimers and trimers are circled with a dashed line in orange, red and purple respectively. The points highlighted in blue are clusters containing 4 monomers, which stand out because of their low O:C ratio. The signal below m/z 300 is due to smaller ionized organic material. (For interpretation of the references to colour in this figure legend, the reader is referred to the Web version of this article.)

3. Results

3.1. Laboratory calibrations of the PSM

3.1.1. Composition of the organic calibration particles

We used the ioniAPi-TOF to confirm the chemical composition of the charged particles produced from β-caryophyllene (BCY) ozonolysis used in the calibration. In Fig. 2, the mass defect plot from the ioniAPi-TOF is shown for two different DMA settings, which had a similar total signal strength in the ioniAPi-TOF. In the upper panel, the DMA was set to −600 V and in the lower panel to −300 V, which corresponds to classified particles of 1.6 nm and 1.2 nm in mobility diameter, respectively, based on previous calibration of the uDMA. The points are coloured by the oxygen to carbon ratio (O:C) and the size is log-scaled with the signal strength of the exact mass. The O:C shows that we have highly oxygenated compounds meaning they are close to what would be found in the atmosphere (Ehn et al., 2014). The monomers, dimers and trimers of BCY HOMs are highlighted in orange, red and purple respectively. The points highlighted in blue are clusters containing 4 monomers. The signal below m/z 300 is due to smaller ionised organic material probably due to impurities, possibly from the DMA sheath flow. In the plot, we see a rather broad mass range even after mobility selection by the DMA. This can partially be due to the resolution of the uDMA. With a resolution of 10–15, the passage of a small range of close or overlapping mobilities of the broad BCY HOM distribution, depending on the concentration of the respective ions, is likely. Classifying an ion of m/z 300 at a resolving power of 10, for example, would mean an m/z range of 150 at half-maximum of the uDMA transmission function whereas at m/z 700 the corresponding m/z range would already be larger than 300. On the other hand, dissociation of cluster ions during transfer from atmospheric pressure into mass spectrometers is commonly observed for different chemical systems and mass spectrometers (Hogan et al., 2010; Passananti et al., 2019; Thomas et al., 2016). Therefore, we conclude that declustering and evaporation on entrance into the ioniAPi-TOF additionally contributes to the observed broad mass range.

3.1.2. Calibration results with the PSM

We calibrated the PSM with BCY oxidation products at two different supersaturation settings using the setup shown in Fig. 1 and compared the results to the standard calibration with tungsten oxide (WOx) particles. The settings of the calibration can be found in Table 1. In Fig. 3, the detection efficiency and activation saturator flow as a function of the particle diameter are displayed. The detection efficiency is calculated from the PSM concentration at the highest saturator flow of 1.3 lpm and the activation saturator flow is defined as the saturator flow rate where 50% of the particles compared to the maximum value are activated and detected by the PSM. We found that, tungsten oxide particles are detected with a higher detection efficiency than BCY oxidation products at the same settings, especially in sizes smaller than 1.7 nm, where the activation probability of organic particles drops quickly. The cut-off diameter for tungsten oxide is 1.2 nm in this calibration, whereas for BCY it is 1.9 nm for the same PSM settings. Next, we increased the saturator temperature to 80°C to increase the supersaturation, until ca. 5 cm^{-3} of homogenous nucleation occurred at 1.3 lpm saturator flow. These counts have not been subtracted for the analysis because they are too small to have an effect on the detection efficiency. Increasing the supersaturation, increases the detection efficiency for BCY oxidation products significantly and decreases the cut-off diameter to 1.7 nm.

In addition, the activation flow rate, which is the flow rate at which half of particles are activated, is affected by the change in chemical composition. It is increasing much quicker with decreasing particle size for BCY oxidation products than for tungsten oxide. For example, 1.9 nm BCY oxidation products are activated at a saturator flow rate around 1.1 lpm, but similarly sized WOx particles already at 0.2 lpm. This shows how important it is to consider the particle composition effect before inferring size information from the

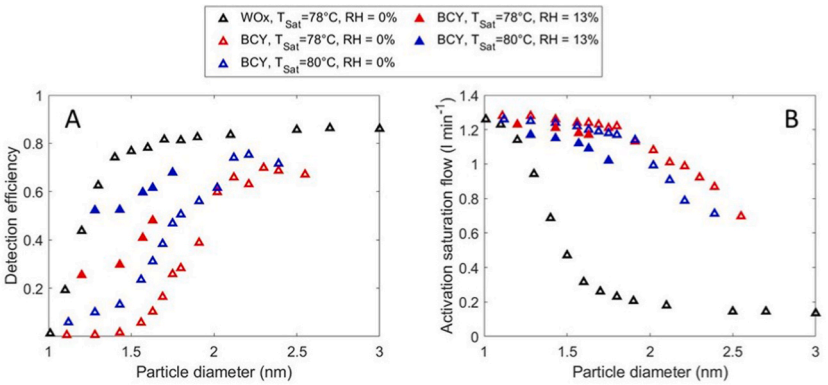

Fig. 3. The detection efficiency (A) and the activation saturator flow (B) of the PSM for positively charged BCY oxidation products at two supersaturation settings compared to negatively charged tungsten oxide calibration. The cut-off diameter for tungsten oxide is 1.2 nm and for BCY oxide 1.9 nm at the same settings in dry conditions. Increasing the saturator temperature by 2°C, increases the detection efficiency and decreases the cut-off diameter to 1.7 nm. Changing the relative humidity to 13%, decreases the cut-off diameter even to 1.6 nm. The activation saturator flow is clearly higher for BCY particles compared to WOx but does not change much with changing humidity or supersaturation. The cut-off diameter for 80°C saturator temperature and 13% humidity is 1.5 nm.

supersaturation scanning method.

3.1.3. Humidity dependency

In the second set of experiments, we increased the absolute humidity from 0.0008 to 4.22 g m^{-3}, which corresponds to a relative humidity of 13% at 31°C (Fig. 3). The detection efficiency increased significantly with increased humidity. The cut-off diameter decreased from 1.9 nm in dry conditions to about 1.6 nm in humid conditions when the saturator temperature was 78°C and from 1.7 nm to 1.5 nm for 80°C. Unfortunately this set of experiments was limited to sizes below 1.7 nm, so the plateau value and activation flow rates could not be determined. Therefore, the cut-off diameter in this experiment could only be estimated. The cut-off diameters of our calibrations are summarised in Table 2. In summary, increasing the relative humidity to 13% has a higher effect on the detection efficiency of BCY oxidation products than increasing the supersaturation of the PSM by increasing the saturator temperature by 2°C. However, in all cases the activation efficiency is clearly lower than for WOx.

In order to investigate this humidity effect in more detail, we conducted another experiment with BCY, where we increased the absolute humidity up to 10 g m^{-3}, which corresponds to 30% relative humidity, in 3 steps (Fig. 4A). At each humidity stage, we set the DMA to select 1.7 nm particles and repeated the calibration at 4 different supersaturation settings by setting the saturator temperature of the PSM to 76°C, 78°C, 80°C and 82°C. For each setting, we also did a measurement where the DMA is set to 0 V, meaning no particles would come through and all counts in the PSM are a result of homogeneous nucleation. Those counts need to be subtracted before the data analysis. The humidity effect was most notable at low supersaturation settings. The detection efficiency doubled for the lowest saturator temperature setting, when we increased the relative humidity by 10%. Increasing the saturator temperature increases the detection efficiency already on its own, therefore the humidity does not increase the detection efficiency as much at higher supersaturation settings. Increasing the humidity also increases the homogeneous nucleation within the PSM. Especially at higher supersaturation settings, the increased humidity causes high homogeneous nucleation (Fig. 4B) that needs to be subtracted, which can lead to errors in the data analysis if it is not accounted for.

These findings agree with Tauber et al. (2019), who looked at humidity effects in butanol based CPCs. They found that increasing the humidity lowers the saturation ratio from butanol on natrium chloride therefore increasing the detection efficiency. Furthermore, Toropainen et al. (2021) found that water molecules are reducing the evaporation rates and therefore stabilising formed clusters of natrium chloride. It is reasonable to assume that humidity does the same for DEG based particle counters, which explains the increased detection efficiency in humid conditions. Another possibility is that the increase in detection efficiency due to humidity could be caused by the water uptake of the particle. This adsorption of water molecules would shift the collision cross section of the particle and make it easier to activate (Thomas et al., 2016). Further measurements are needed to determine the exact reason for the increased detection efficiency.

3.2. Composition dependence of the cut-off diameter during CLOUD experiments

In the CLOUD experiments, particle formation rates are calculated for 1.7 nm particles (Kirkby et al., 2011). Therefore, we wanted to determine the saturator flow rate at which the PSM cut-off size best corresponds to 1.7 nm for particles of different chemical compositions. For doing that, we compared the PSM measurements at nominal 1.7 nm cut-off size, based on WOx calibration, to cumulated concentrations at different size channels of the NAIS using the method described in Section 2.4 and equation (1). Since the NAIS measurement is not composition dependent, it is used as a reference instrument in this case (Mirme et al., 2013). Note, that this cross calibration method can be applied to other diameters as well. In Fig. 5, an example of this comparison is shown. The concentrations of PSM and NAIS are normalised to the maximum concentration detected in each size class to be able to compare the time evolution of the different size bins. We collected data during experiments, where iodine, α-pinene or β-caryophyllene were used as precursors of particle formation, as well as mixtures of α-pinene and isoprene. The results are summarised in Table 3.

During the iodine experiments, when particle formation proceeds via clustering of iodine oxoacids (He et al., 2021; Sipilä et al., 2016), the appearance times of ions detected by PSM and NAIS agreed well (Fig. 5A). We defined the appearance time as the time when 50% of the normalised concentration was reached (Lehtipalo et al., 2014).The normalised ion concentration of the PSM at nominal 1.7 nm cut-off size is comparable to the normalised concentration of ions detected by NAIS at the same size. However, during the organic runs with pure α-pinene or β-caryophyllene as precursors, the nominal 1.7 nm channel of the PSM ion concentration usually fell between the 1.9 nm and 2.06 nm channel of the NAIS, suggesting, a +0.3 nm (±0.1 nm) diameter shift in the cut-off diameter (Fig. 5B-C). In addition, mixtures of organics like α-pinene and isoprene had the same behaviour, probably because of the similar

Table 2
Summary of the cut-off diameter of the different calibrations.

Compound	Humidity	PSM setting	Cut-off diameter
Tungsten oxidation products	0%	T_{Sat} = 78°C	1.2 nm
BCY oxidation products	0%	T_{Sat} = 78°C	1.9 nm
BCY oxidation products	0%	T_{Sat} = 80°C	1.7 nm
BCY oxidation products	13%	T_{Sat} = 78°C	1.6 nm
BCY oxidation products	13%	T_{Sat} = 80°C	1.5 nm

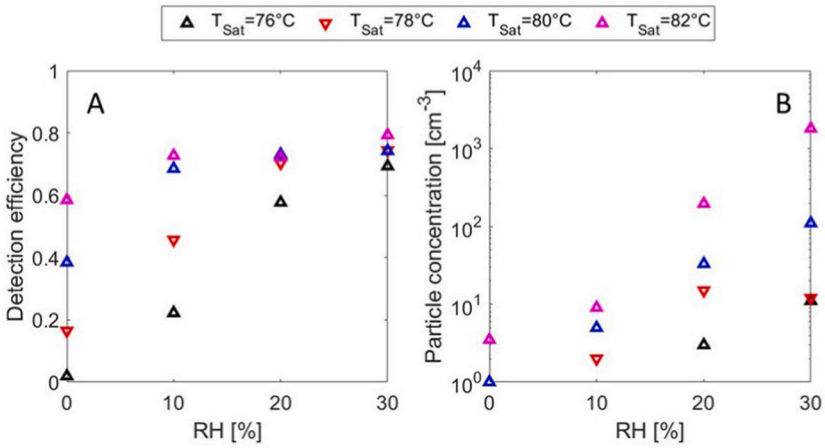

Fig. 4. The detection efficiency of 1.7 nm positively charged BCY oxidation products at multiple relative humidities and supersaturation settings (A) and the particle concentration caused by homogeneous nucleation at the same settings (B). Plot A shows that the detection efficiency increases significantly with increasing humidity in the Teflon bag, most significantly between 0 and 10%. Increasing the humidity also increases the homogeneous nucleation, especially at higher supersaturation settings. The points are coloured by saturator temperature to represent the different supersaturation settings of the PSM. There was no homogeneous nucleation for 0% RH at 76°C and 78°C and also for 10% RH at 76°C.

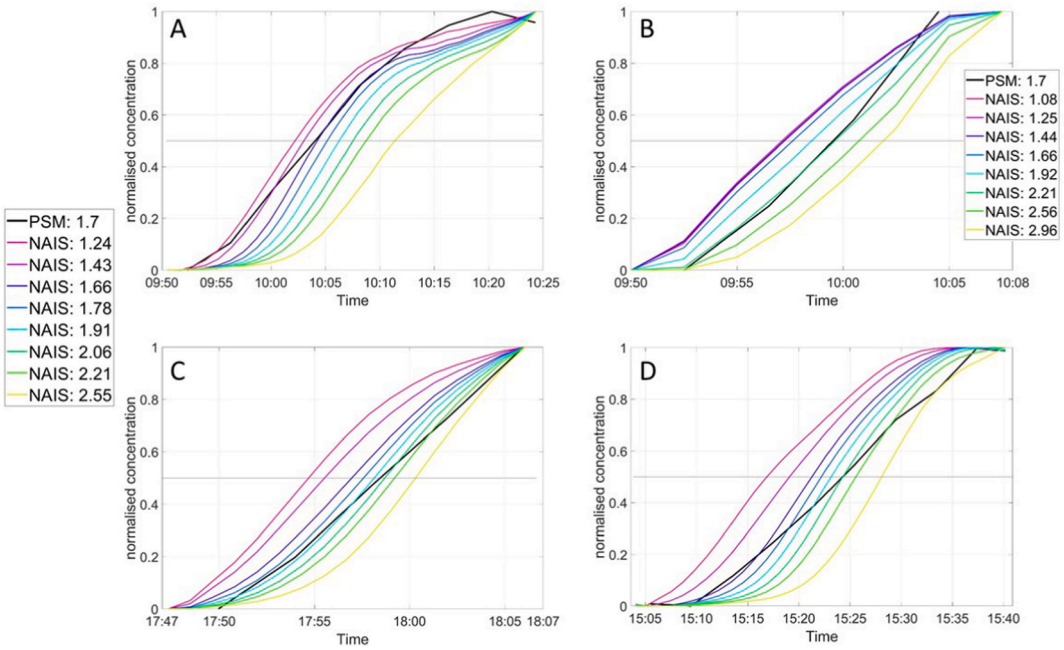

Fig. 5. The normalised ion concentration detected by the PSM at nominal 1.7 nm cut-off size (black) compared to cumulated concentrations above a certain size channel of the NAIS during new particle formation experiment in the CLOUD chamber. The different lines refer to the different mobility diameters in nm. In the case of iodine nucleation (A), the appearance times of the ions in the PSM agree well with the NAIS, suggesting similar cut-off size. Whereas in the case of β-caryophyllene (B), α-pinene (C) and α-pinene-isoprene (D) nucleation the PSM cut-off size is shifted. Note that B has a different legend because a different NAIS model was used. For α-pinene and α-pinene-isoprene nucleation, it falls between 1.91 nm and 2.06 nm and for β-caryophyllene between 1.92 and 2.21 nm of the NAIS. We conclude from this, that the real cut-off size in the PSM is about 2.0 nm ± 0.1 nm for those cases. Therefore a +0.3 nm (±0.1 nm) shift can be observed compared to the tungsten oxide calibration.

Table 3
Cut-off diameter shift (nm) for different experiments. The humidity was stable for each run but several examples were used.

Particle formation precursor	RH	Diameter change relative to WOx calibration
Iodine	20–70%	0 (±0.1 nm)
α-pinene	40–80%	0.3 (±0.1 nm)
β-caryophyllene	40%	0.3 (±0.1 nm)
α-pinene/isoprene	40–80%	0.3 (±0.1 nm)
BCY (lab, low SS)	0%	0.7 nm
BCY (lab, high SS)	0%	0.5 nm
BCY(lab, low SS)	13%	0.4 nm

composition of the growing particles (Fig. 5D). This shift is significantly smaller than what we saw in calibrations under dry conditions in the lab, but the CLOUD experiments were always conducted with 20% relative humidity or higher. The diameter shift between the tungsten oxide calibration and the calibration with BCY at 13% relative humidity is +0.4 nm and therefore agrees with the CLOUD results.

4. Conclusion

We characterised the PSM with atmospherically relevant organic particles and determined the shift of the cut-off size relative to the standard calibration done with tungsten oxide. We can confirm the results of earlier studies (Kangasluoma et al., 2014) showing that the PSM detects organic particles less efficiently than inorganic ones. The cut-off diameter for BCY oxidation products is 1.9 nm and for tungsten oxide at 1.2 nm in dry conditions (RH = 0%) with the same PSM settings. Nevertheless, increasing the saturation ratio of DEG or the relative humidity increased the detection efficiency significantly. However, as the homogenous nucleation background also increases with supersaturation and relative humidity, one should carefully characterise the instrument to find the optimal setting.

In the CLOUD experiments, we produced particles from the oxidation of different organic precursors, such as α-pinene, BCY and isoprene, as well as iodine. We compared the appearance times of different sized ions measured with the PSM to the ions detected with the NAIS, which is not affected by changes in ion composition. This led to the results that the organic mixtures have a cut-off shift of +0.3 nm (±0.1 nm) at relative humidities higher than 30% compared to the tungsten oxide calibration, whereas in experiments with iodine the two instruments agreed and no cut-off shift was observed.

It is important to know the chemical composition of the measured particles to determine information that depends on the cut-off size, such as the size distribution and to calculate formation rates accurately. Under ideal circumstances, the PSM should be calibrated with similar humidity and particle composition as it is expected to measure in the field. However, the results in this study can be used to correct for humidity and chemical composition effects in the data analysis.

Declaration of competing interest

The authors declare that they have no known competing financial interests or personal relationships that could have appeared to influence the work reported in this paper.

Acknowledgements

This work has received funding from the European Union's Horizon 2020 research and innovation programme under the Marie Skłodowska-Curie grant agreement No 764991 (CLOUD-MOTION). We also acknowledge the following projects: ACCC Flagship funded by the Academy of Finland grant number 337549, Academy professorship funded by the Academy of Finland (grant no. 302958), Russian Mega Grant project "Megapolis - heat and pollution island: interdisciplinary hydroclimatic, geochemical and ecological analysis" application reference 2020-220-08-5835, "Quantifying carbon sink, CarbonSink+ and their interaction with air quality" INAR project funded by Jane and Aatos Erkko Foundation, European Research Council (ERC) project ATM-GTP Contract No. 742206.

References

Albrecht, B. A. (1989). Aerosols, cloud microphysics, and fractional cloudiness. *Science, 245*(4923), 1227–1230.
Attoui, M. (2018). Activation of sub 2 nm singly charged particles with butanol vapors in a boosted 3776 TSI CPC. *Journal of Aerosol Science, 126*, 47–57.
Bauer, S. E., & Menon, S. (2012). Aerosol direct, indirect, semidirect, and surface albedo effects from sector contributions based on the IPCC AR5 emissions for preindustrial and present-day conditions. *Journal of Geophysical Research: Atmospheres, 117*(D1).
Breitenlechner, M., Fischer, L., Hainer, M., Heinritzi, M., Curtius, J., & Hansel, A. (2017). PTR3: An instrument for studying the lifecycle of reactive organic carbon in the atmosphere. *Analytical Chemistry, 89*(11), 5824–5831.
Brilke, S., Fölker, N., Kandler, K., Ma, N., Müller, T., Peischl, J., Philipp, A., Seibert, P., Weinzierl, B., & Winkler, P. (2019). *New particle formation and sub-10 nm size distribution measurements in paphos, Cyprus, during the A-LIFE field experiment.* Paper presented at the AGU Fall Meeting Abstracts.
Dada, L., Lehtipalo, K., Kontkanen, J., Nieminen, T., Baalbaki, R., Ahonen, L., Duplissy, J., Yan, C., Chu, B., & Petäjä, T. (2020). Formation and growth of sub-3-nm aerosol particles in experimental chambers. *Nature Protocols, 15*(3), 1013–1040.
Duplissy, J., Merikanto, J., Franchin, A., Tsagkogeorgas, G., Kangasluoma, J., Wimmer, D., Vuollekoski, H., Schobesberger, S., Lehtipalo, K., & Flagan, R. (2016). Effect of ions on sulfuric acid-water binary particle formation: 2. Experimental data and comparison with QC-normalized classical nucleation theory. *Journal of Geophysical Research: Atmospheres, 121*(4), 1752–1775.

Ehn, M., Thornton, J. A., Kleist, E., Sipilä, M., Junninen, H., Pullinen, I., Springer, M., Rubach, F., Tillmann, R., & Lee, B. (2014). A large source of low-volatility secondary organic aerosol. *Nature, 506*(7489), 476–479.
Hansel, A., Scholz, W., Mentler, B., Fischer, L., & Berndt, T. (2018). Detection of RO2 radicals and other products from cyclohexene ozonolysis with NH4+ and acetate chemical ionization mass spectrometry. *Atmospheric Environment, 186*, 248–255.
He, X.-C., Tham, Y. J., Dada, L., Wang, M., Finkenzeller, H., Stolzenburg, D., Iyer, S., Simon, M., Kürten, A., & Shen, J. (2021). Role of iodine oxoacids in atmospheric aerosol nucleation. *Science, 371*(6529), 589–595.
Hogan, C. J., & De La Mora, J. F. (2010). Ion-pair evaporation from ionic liquid clusters. *Journal of the American Society for Mass Spectrometry, 21*(8), 1382–1386.
Iida, K., Stolzenburg, M. R., & McMurry, P. H. (2009). Effect of working fluid on sub-2 nm particle detection with a laminar flow ultrafine condensation particle counter. *Aerosol Science and Technology, 43*(1), 81–96. https://doi.org/10.1080/02786820802488194
Ito, E., Seto, T., Otani, Y., & Sakurai, H. (2011). Nucleation of ethylene glycol vapor and growth of sub-10-nm particles in nanoparticle size magnifier. *Aerosol Science and Technology, 45*(10), 1250–1259.
Jiang, J., Zhao, J., Chen, M., Eisele, F. L., Scheckman, J., Williams, B. J., Kuang, C., & McMurry, P. H. (2011). First measurements of neutral atmospheric cluster and 1–2 nm particle number size distributions during nucleation events. *Aerosol Science and Technology, 45*(4), ii–v.
Jokinen, T., Kausiala, O., Garmash, O., Peräkylä, O., Junninen, H., Schobesberger, S., Yan, C., Sipilä, M., & Rissanen, M. P. (2016). *Production of highly oxidized organic compounds from ozonolysis of beta-caryophyllene: Laboratory and field measurements*. Boreal Environment Research.
Kangasluoma, J., Attoui, M., Junninen, H., Lehtipalo, K., Samodurov, A., Korhonen, F., Sarnela, N., Schmidt-Ott, A., Worsnop, D., & Kulmala, M. (2015a). Sizing of neutral sub 3 nm tungsten oxide clusters using Airmodus Particle Size Magnifier. *Journal of Aerosol Science, 87*, 53–62.
Kangasluoma, J., Cai, R., Jiang, J., Deng, C., Stolzenburg, D., Ahonen, L. R., Chan, T., Fu, Y., Kim, C., & Laurila, T. M. (2020). Overview of measurements and current instrumentation for 1–10 nm aerosol particle number size distributions. *Journal of Aerosol Science*, 105584.
Kangasluoma, J., Franchin, A., Duplissy, J., Ahonen, L., Korhonen, F., Attoui, M., Mikkilä, J., Lehtipalo, K., Vanhanen, J., & Kulmala, M. (2015b). Operation of the Airmodus A11 nano Condensation Nucleus Counter at various inlet pressures, various operation temperatures and design of a new inlet system. *Atmospheric Measurement Techniques Discussions*.
Kangasluoma, J., Junninen, H., Lehtipalo, K., Mikkilä, J., Vanhanen, J., Attoui, M., Sipilä, M., Worsnop, D., Kulmala, M., & Petäjä, T. (2013). Remarks on ion generation for CPC detection efficiency studies in sub-3-nm size range. *Aerosol Science and Technology, 47*(5), 556–563.
Kangasluoma, J., Kuang, C., Wimmer, D., Rissanen, M., Lehtipalo, K., Ehn, M., Worsnop, D., Wang, J., Kulmala, M., & Petäjä, T. (2014). Sub-3 nm particle size and composition dependent response of a nano-CPC battery. *Atmospheric Measurement Techniques, 7*(3), 689.
Kangasluoma, J., Samodurov, A., Attoui, M., Franchin, A., Junninen, H., Korhonen, F., Kurtén, T., Vehkamäki, H., Sipilä, M., & Lehtipalo, K. (2016). Heterogeneous nucleation onto ions and neutralized ions: Insights into sign-preference. *Journal of Physical Chemistry C, 120*(13), 7444–7450.
Keshavarz, F., Kurtén, T., Vehkamäki, H., & Kangasluoma, J. (2020). Seed–adsorbate interactions as the key of heterogeneous butanol and diethylene glycol nucleation on ammonium bisulfate and tetramethylammonium bromide. *The Journal of Physical Chemistry A*.
Kim, K.-H., Kabir, E., & Kabir, S. (2015). A review on the human health impact of airborne particulate matter. *Environment International, 74*, 136–143.
Kim, C. S., Okuyama, K., & de la Mora, J. F. (2003). Performance evaluation of an improved particle size magnifier (PSM) for single nanoparticle detection. *Aerosol Science & Technology, 37*(10), 791–803.
Kirkby, J., Curtius, J., Almeida, J., Dunne, E., Duplissy, J., Ehrhart, S., Franchin, A., Gagné, S., Ickes, L., & Kürten, A. (2011). Role of sulphuric acid, ammonia and galactic cosmic rays in atmospheric aerosol nucleation. *Nature, 476*(7361), 429–433.
Kirkby, J., Duplissy, J., Sengupta, K., Frege, C., Gordon, H., Williamson, C., Heinritzi, M., Simon, M., Yan, C., & Almeida, J. (2016). Ion-induced nucleation of pure biogenic particles. *Nature, 533*(7604), 521–526.
Kogan, Y. I., & Burnasheva, Z. (1960). Growth and measurement of condensation nuclei in a continuous stream. *Zhurnal Fizicheskoi Khimii, 34*(12), 2630–2639.
Kuang, C., Chen, M., McMurry, P. H., & Wang, J. (2012). Modification of laminar flow ultrafine condensation particle counters for the enhanced detection of 1 nm condensation nuclei. *Aerosol Science and Technology, 46*(3), 309–315.
Kulmala, M., Kontkanen, J., Junninen, H., Lehtipalo, K., Manninen, H. E., Nieminen, T., Petäjä, T., Sipilä, M., Schobesberger, S., & Rantala, P. (2013). Direct observations of atmospheric aerosol nucleation. *Science, 339*(6122), 943–946.
Kulmala, M., Petäjä, T., Nieminen, T., Sipilä, M., Manninen, H. E., Lehtipalo, K., Dal Maso, M., Aalto, P. P., Junninen, H., & Paasonen, P. (2012). Measurement of the nucleation of atmospheric aerosol particles. *Nature Protocols, 7*(9), 1651–1667.
Lehtipalo, K., Leppa, J., Kontkanen, J., Kangasluoma, J., Franchin, A., Wimnner, D., Schobesberger, S., Junninen, H., Petaja, T., & Sipila, M. (2014). *Methods for determining particle size distribution and growth rates between 1 and 3 nm using the Particle Size Magnifier*. Boreal Environment Research.
Lehtipalo, K., Yan, C., Dada, L., Bianchi, F., Xiao, M., Wagner, R., Stolzenburg, D., Ahonen, L. R., Amorim, A., & Baccarini, A. (2018). Multicomponent new particle formation from sulfuric acid, ammonia, and biogenic vapors. *Science Advances, 4*(12). eaau5363.
Leiminger, M., Feil, S., Mutschlechner, P., Ylisirniö, A., Gunsch, D., Fischer, L., Jordan, A., Schobesberger, S., Hansel, A., & Steiner, G. (2019). Characterisation of the transfer of cluster ions through an atmospheric pressure interface time-of-flight mass spectrometer with hexapole ion guides. *Atmospheric Measurement Techniques, 12*(10), 5231–5246.
Manninen, H. (2011). *Direct detection of atmospheric particle formation using the Neutral cluster and Air Ion Spectrometer*.
Manninen, H., Mirme, S., Mirme, A., Petäjä, T., & Kulmala, M. (2016). How to reliably detect molecular clusters and nucleation mode particles with Neutral cluster and Air Ion Spectrometer (NAIS). *Atmospheric Measurement Techniques, 9*(8), 3577–3605.
McMurry, P. H. (2000). The history of condensation nucleus counters. *Aerosol Science & Technology, 33*(4), 297–322.
Merikanto, J., Spracklen, D., Mann, G., Pickering, S., & Carslaw, K. (2009). Impact of nucleation on global CCN. *Atmospheric Chemistry and Physics Discussions, 9*(3).
Mirme, S., & Mirme, A. (2013). The mathematical principles and design of the NAIS-a spectrometer for the measurement of cluster ion and nanometer aerosol size distributions. *Atmospheric Measurement Techniques, 6*(4), 1061.
Okuyama, K., Kousaka, Y., & Motouchi, T. (1984). Condensational growth of ultrafine aerosol particles in a new particle size magnifier. *Aerosol Science and Technology, 3*(4), 353–366.
Passananti, M., Zapadinsky, E., Zanca, T., Kangasluoma, J., Myllys, N., Rissanen, M. P., Kurtén, T., Ehn, M., Attoui, M., & Vehkamäki, H. (2019). How well can we predict cluster fragmentation inside a mass spectrometer? *Chemical Communications, 55*(42), 5946–5949.
Patel, S., Sankhyan, S., Boedicker, E. K., DeCarlo, P. F., Farmer, D. K., Goldstein, A. H., Katz, E. F., Nazaroff, W. W., Tian, Y., & Vanhanen, J. (2020). Indoor particulate matter during HOMEChem: Concentrations, size distributions, and exposures. *Environmental Science & Technology, 54*(12), 7107–7116.
Peineke, C., Attoui, M., & Schmidt-Ott, A. (2006). Using a glowing wire generator for production of charged, uniformly sized nanoparticles at high concentrations. *Journal of Aerosol Science, 37*(12), 1651–1661.
Picard, D., Attoui, M., & Sellegri, K. (2019). B3010: A boosted TSI 3010 condensation particle counter for airborne studies. *Atmospheric Measurement Techniques, 12*(4), 2531–2543.
Schmidt-Ott, A., Schurtenberger, P., & Siegmann, H. (1980). Enormous yield of photoelectrons from small particles. *Physical Review Letters, 45*(15), 1284.
Seto, T., Okuyama, K., De Juan, L., & Fernandez de la Mora, J. (1997). Condensation of supersaturated vapors on monovalent and divalent ions of varying size. *The Journal of Chemical Physics, 107*(5), 1576–1585.
Sgro, L. A., & Fernández de la Mora, J. (2004). A simple turbulent mixing CNC for charged particle detection down to 1.2 nm. *Aerosol Science and Technology, 38*(1), 1–11.
Sipilä, M., Sarnela, N., Jokinen, T., Henschel, H., Junninen, H., Kontkanen, J., Richters, S., Kangasluoma, J., Franchin, A., & Peräkylä, O. (2016). Molecular-scale evidence of aerosol particle formation via sequential addition of HIO 3. *Nature, 537*(7621), 532–534.
Stabile, L., Dell'Isola, M., Frattolillo, A., Massimo, A., & Russi, A. (2016). Effect of natural ventilation and manual airing on indoor air quality in naturally ventilated Italian classrooms. *Building and Environment, 98*, 180–189.
Steiner, G., Attoui, M., Wimmer, D., & Reischl, G. (2010). A medium flow, high-resolution Vienna DMA running in recirculating mode. *Aerosol Science and Technology, 44*(4), 308–315.

Sulo, J., Sarnela, N., Kontkanen, J., Ahonen, L., Paasonen, P., Laurila, T., Jokinen, T., Kangasluoma, J., Petäjä, T., & Kulmala, M. (2020). Long-term measurement of sub-3nm particles and their precursor gases in the boreal forest. *Atmospheric Chemistry and Physics Discussions*, 1–38.

Tauber, C., Brilke, S., Wlasits, P. J., Bauer, P. S., Köberl, G., Steiner, G., & Winkler, P. M. (2019). Humidity effects on the detection of soluble and insoluble nanoparticles in butanol operated condensation particle counters. *Atmospheric Measurement Techniques, 12*(7), 3659–3671.

Thomas, J. M., He, S., Larriba-Andaluz, C., DePalma, J. W., Johnston, M. V., & Hogan, C. J., Jr. (2016). Ion mobility spectrometry-mass spectrometry examination of the structures, stabilities, and extents of hydration of dimethylamine–sulfuric acid clusters. *Physical Chemistry Chemical Physics, 18*(33), 22962–22972.

Toropainen, A., Kangasluoma, J., Kurtén, T., Vehkamäki, H., Keshavarz, F., & Kubecka, J. (2021). Heterogeneous nucleation of butanol on NaCl: A computational study of temperature, humidity, seed charge, and seed size effects. *The Journal of Physical Chemistry A, 125*(14), 3025–3036.

Vanhanen, J., Mikkilä, J., Lehtipalo, K., Sipilä, M., Manninen, H., Siivola, E., Petäjä, T., & Kulmala, M. (2011). Particle size magnifier for nano-CN detection. *Aerosol Science and Technology, 45*(4), 533–542.

Wagner, R., Manninen, H. E., Franchin, A., Lehtipalo, K., Mirme, S., Steiner, G., Petäjä, T., & Kulmala, M. (2016). *On the accuracy of ion measurements using a Neutral cluster and Air Ion Spectrometer*.

Wagner, R., Yan, C., Lehtipalo, K., Duplissy, J., Nieminen, T., Kangasluoma, J., Ahonen, L. R., Dada, L., Kontkanen, J., & Manninen, H. E. (2017). The role of ions in new particle formation in the CLOUD chamber. *Atmospheric Chemistry and Physics, 17*(24), 15181–15197.

Wang, X., Caldow, R., Sem, G. J., Hama, N., & Sakurai, H. (2010). Evaluation of a condensation particle counter for vehicle emission measurement: Experimental procedure and effects of calibration aerosol material. *Journal of Aerosol Science, 41*(3), 306–318.

Wang, Z., Wu, Z., Yue, D., Shang, D., Guo, S., Sun, J., Ding, A., Wang, L., Jiang, J., & Guo, H. (2017). New particle formation in China: Current knowledge and further directions. *The Science of the Total Environment, 577*, 258–266.

Wiedensohler, A., Wiesner, A., Weinhold, K., Birmili, W., Hermann, M., Merkel, M., Müller, T., Pfeifer, S., Schmidt, A., & Tuch, T. (2018). Mobility particle size spectrometers: Calibration procedures and measurement uncertainties. *Aerosol Science and Technology, 52*(2), 146–164.

Wimmer, D., Lehtipalo, K., Franchin, A., Kangasluoma, J., Kreissl, F., Kürten, A., Kupc, A., Metzger, A., Mikkilä, J., & Petäjä, T. (2013). Performance of diethylene glycol-based particle counters in the sub-3 nm size range. *Atmospheric Measurement Techniques, 6*(7), 1793–1804.

Winklmayr, W., Reischl, G., Lindner, A., & Berner, A. (1991). A new electromobility spectrometer for the measurement of aerosol size distributions in the size range from 1 to 1000 nm. *Journal of Aerosol Science, 22*(3), 289–296.

Wlasits, P. J., Stolzenburg, D., Tauber, C., Brilke, S., Schmitt, S. H., Winkler, P. M., & Wimmer, D. (2020). Counting on chemistry: Laboratory evaluation of seed-material-dependent detection efficiencies of ultrafine condensation particle counters. *Atmospheric Measurement Techniques, 13*(7), 3787–3798.

Woo, K., Chen, D., Pui, D., & McMurry, P. H. (2001). Measurement of Atlanta aerosol size distributions: Observations of ultrafine particle events. *Aerosol Science & Technology, 34*(1), 75–87.

Yli-Ojanperä, J., Sakurai, H., Iida, K., Mäkelä, J. M., Ehara, K., & Keskinen, J. (2012). Comparison of three particle number concentration calibration standards through calibration of a single CPC in a wide particle size range. *Aerosol Science and Technology, 46*(11), 1163–1173.